

Self-assembly of a layered two-dimensional molecularly woven fabric

<https://doi.org/10.1038/s41586-020-3019-9>

Received: 1 July 2020

Accepted: 28 October 2020

Published online: 16 December 2020

 Check for updates

David P. August¹, Robert A. W. Dryfe^{1,2}, Sarah J. Haigh³, Paige R. C. Kent¹, David A. Leigh^{1✉}, Jean-François Lemonnier¹, Zheling Li³, Christopher A. Muryn¹, Leoni I. Palmer¹, Yiwei Song¹, George F. S. Whitehead¹ & Robert J. Young³

Fabrics—materials consisting of layers of woven fibres—are some of the most important materials in everyday life¹. Previous nanoscale weaves^{2–16} include isotropic crystalline covalent organic frameworks^{12–14} that feature rigid helical strands interlaced in all three dimensions, rather than the two-dimensional^{17,18} layers of flexible woven strands that give conventional textiles their characteristic flexibility, thinness, anisotropic strength and porosity. A supramolecular two-dimensional kagome weave¹⁵ and a single-layer, surface-supported, interwoven two-dimensional polymer¹⁶ have also been reported. The direct, bottom-up assembly of molecular building blocks into linear organic polymer chains woven in two dimensions has been proposed on a number of occasions^{19–23}, but has not previously been achieved. Here we demonstrate that by using an anion and metal ion template, woven molecular ‘tiles’ can be tessellated into a material consisting of alternating aliphatic and aromatic segmented polymer strands, interwoven within discrete layers. Connections between slowly precipitating pre-woven grids, followed by the removal of the ion template, result in a wholly organic molecular material that forms as stacks and clusters of thin sheets—each sheet up to hundreds of micrometres long and wide but only about four nanometres thick—in which warp and weft single-chain polymer strands remain associated through periodic mechanical entanglements within each sheet. Atomic force microscopy and scanning electron microscopy show clusters and, occasionally, isolated individual sheets that, following demetallation, have slid apart from others with which they were stacked during the tessellation and polymerization process. The layered two-dimensional molecularly woven material has long-range order, is birefringent, is twice as stiff as the constituent linear polymer, and delaminates and tears along well-defined lines in the manner of a macroscopic textile. When incorporated into a polymer-supported membrane, it acts as a net, slowing the passage of large ions while letting smaller ions through.

Metal template synthesis is a powerful tool for directing the assembly of difficult-to-obtain molecular-level architectures, such as the ordered entanglements necessary for molecular knots, links and other entwined structures^{24–35}. In principle, it should be possible to tessellate pre-woven metal-coordinated molecular grids in two dimensions to form a woven molecular material^{20,21}. However, so far, grids featuring woven—rather than stacked^{36,37}—ligand strands have not been reported (other than the simplest, 2×2 , arrangement, which does not have internal crossings). We recently prepared a metal-coordinated interwoven 3×3 molecular grid, $[\text{Fe}_9\mathbf{1}_6](\text{BF}_4)_{18}$, as an intermediate in the synthesis of a molecular 7₄ knot³⁸ (Fig. 1a). Each ligand strand (**1**) contains three tridentate sites for the octahedral Fe(II) ions, separated by thiazolo[5,4-*d*]thiazole groups (Fig. 1a). The metal ion coordination promotes strand crossings in the pattern required for such a knot, while the X-ray crystal structure of

$[\text{Fe}_9\mathbf{1}_6](\text{BF}_4)_{18}$ (Fig. 1b–d) indicates a template effect of the BF_4^- anions arising from the stabilization of the orthogonal arrangement of the woven ligand strands through a combination of charge–dipole ($\text{Fe}(\text{II}) \cdots \text{F}-\text{B}$) and anion– π ($[\text{F}_3\text{B}-\text{F}] \cdots \text{thiazole}$) interactions (Fig. 1b). The crystal packing of $[\text{Fe}_9\mathbf{1}_6](\text{BF}_4)_{18}$ features layers of $[\text{Fe}_9\mathbf{1}_6]^{18+}$ grids (each with four encapsulated BF_4^- anions) with all of the ligand strands running parallel or orthogonal to the other strands in the same layer (Fig. 1c). The grid planes are separated by sheets of the remaining BF_4^- anions (Fig. 1d). Within each grid layer, the molecules are arranged in squares with the strand ends pointing across the squares towards, but slightly offset from, the strand ends of the grid opposite (Fig. 1c).

The fortuitous solid-state arrangement of $[\text{Fe}_9\mathbf{1}_6](\text{BF}_4)_{18}$ (discrete layers, horizontally offset layers, tiled arrangement of interwoven grids, parallel arrays of strands) suggested that connecting the strand end

¹Department of Chemistry, University of Manchester, Manchester, UK. ²Henry Royce Institute, University of Manchester, Manchester, UK. ³Department of Materials, National Graphene Institute, University of Manchester, Manchester, UK. ✉e-mail: david.leigh@manchester.ac.uk

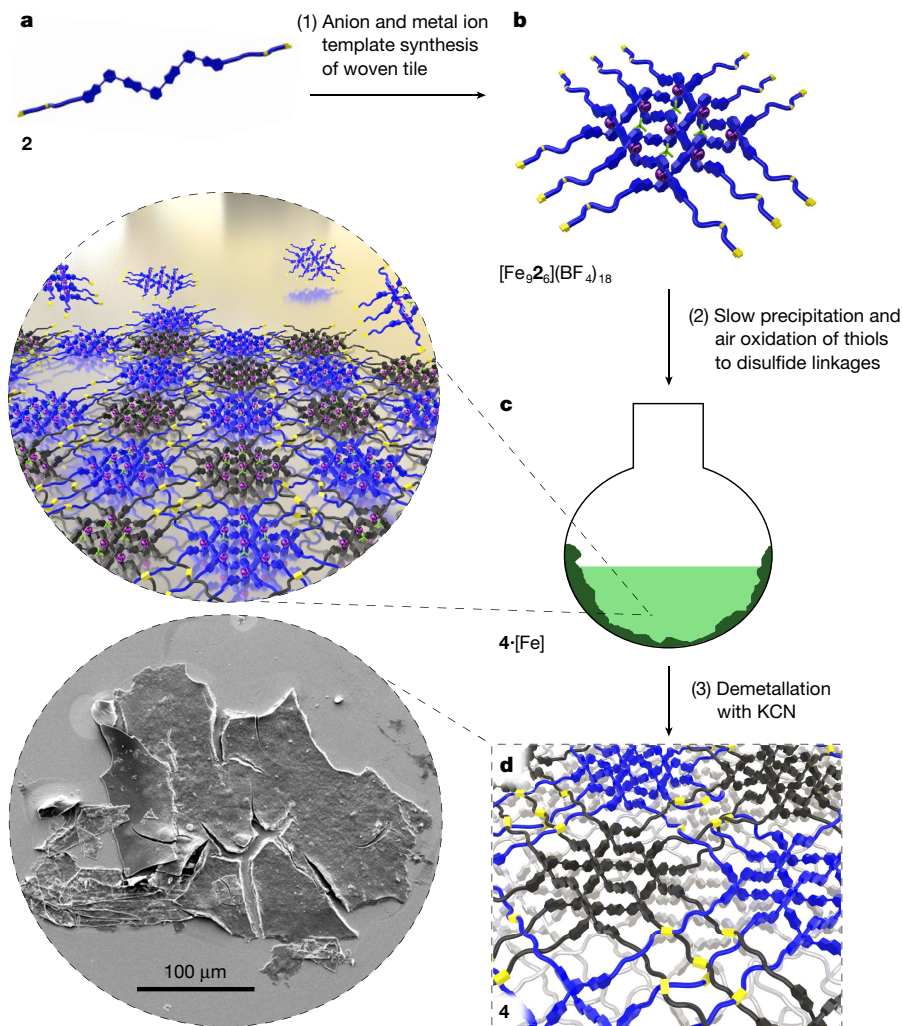


Fig. 2 | Bottom-up self-assembly of layered 2D molecularly woven fabric 4. **a**, Strand **2**, a ligand with thiol end groups. **b**, Formation of 3×3 interwoven grid $[\text{Fe}_9\text{2}_6](\text{BF}_4)_{18}$ —a ‘woven tile’—by anion and metal ion template weaving of **2**. **c**, Slow precipitation of $[\text{Fe}_9\text{2}_6](\text{BF}_4)_{18}$ and air oxidation of the thiol groups to disulfide bonds. The inset depicts assembly of the already woven tiles into 2D layers, $4 \cdot [\text{Fe}]$. Grids are coloured blue and grey to clarify the weaving pattern. As oxidation in solution is slow, most of the disulfide linkages probably form in the solid state. **d**, Treatment of $4 \cdot [\text{Fe}]$ with excess KCN removes the template salts to afford a wholly organic molecularly woven fabric, **4**, as stacked sheets and clusters, with individual sheets having typical dimensions up to several hundreds of micrometres in length and width but only a few nanometres thick. Delamination (sliding of one sheet over another, for example, Fig. 3d) indicates

the mechanical entanglements within each layer. Two key features of the X-ray crystal structure of $[\text{Fe}_9\text{1}_6](\text{BF}_4)_{18}$ are the planes of the anions and the bulky isopentyl groups between grid layers, and the horizontal approximately 1.8 nm offset in grids (Fig. 1c) that alternates between the *a* and *b* axis for each pair of layers. With appropriate length linkers, these features should prevent the formation of strand connections between layers that would otherwise result in a 3D crosslinked material.

Synthesis of 3 and 4

To promote intergrid connections of the end groups, we used chemistry known to be effective in condensed matter—specifically the oxidation of thiols to disulfides, a reaction commonly used to crosslink proteins and other polymers³⁹. A useful feature of this reaction is that the only reagent, O_2 , and the waste product, H_2O , should both be able to readily

diffuse through the material. Treatment of **1** with 1,3-propanedithiol ($\text{HS}(\text{CH}_2)_3\text{SH}$) and 2,2'-azobis(2-methylpropionitrile) (AIBN) in dichloromethane in a sealed vial at 80°C afforded the dithiol building block, **2**, in near-quantitative yield through a thiol-ene ‘click’ reaction (Fig. 1a, step 1). Treatment of **2** with $\text{Fe}(\text{BF}_4)_2 \cdot 6\text{H}_2\text{O}$ (1.5 equiv.) in toluene:acetonitrile (3:5) at 120°C in a sealed vial under microwave irradiation for 20 h generated $[\text{Fe}_9\text{2}_6](\text{BF}_4)_{18}$ in 62% yield (Fig. 1a, step 3, Supplementary Video 1). Electrospray ionization mass spectrometry (ESI-MS) showed multiply charged ions, $\{[\text{Fe}_9\text{2}_6](\text{BF}_4)_n\}^{(18-n)+}$ ($n = 7-11$), corresponding to the loss of BF_4^- counterions from the 3×3 grid (Supplementary Fig. 3). The thiol-terminated grid oxidized in air: ESI-MS and ^1H nuclear magnetic resonance (NMR) spectroscopy showed slow loss of the thiol protons and the formation of some intragrid disulfide linkages in dilute solution over the course of a few days (Supplementary Fig. 5); in the solid state, oxidation was complete within a few hours as

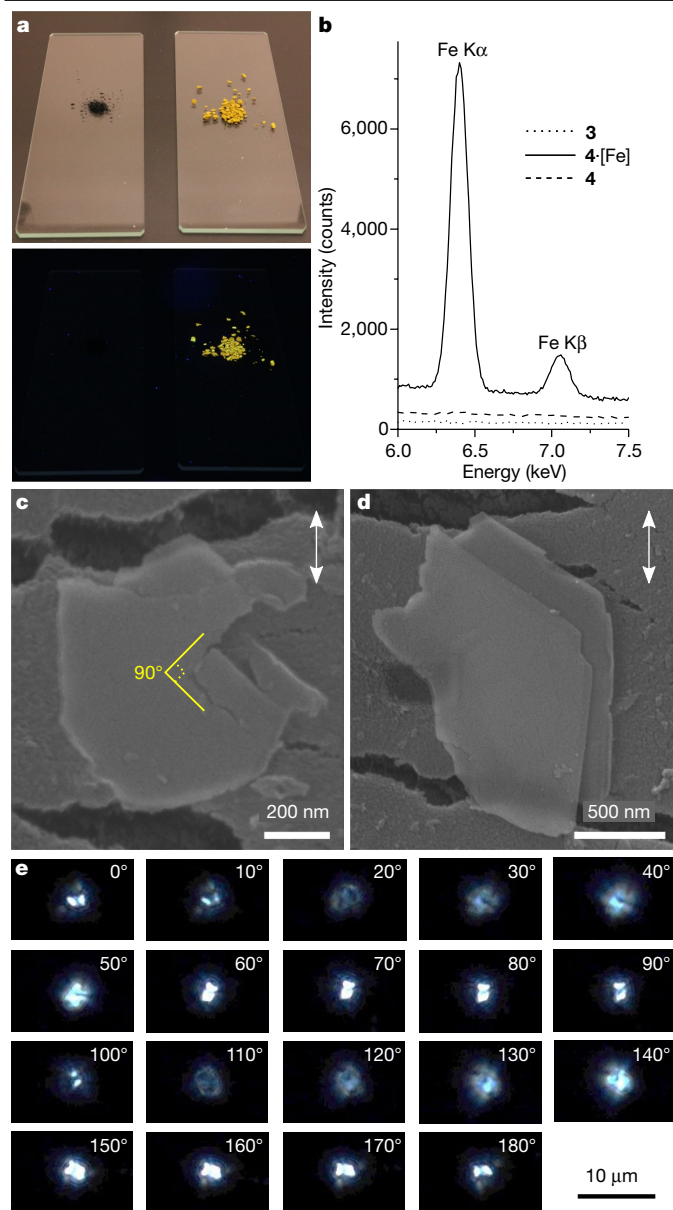


Fig. 3 | Images of layered 2D molecularly woven fabric 4, and evidence for long-range order. **a**, Top: image of the 2D molecularly woven polymer, with metal salt still incorporated (**4**·[Fe], left) and demetallated and ion free (**4**, right). Bottom: the same samples in the dark under ultraviolet irradiation, showing fluorescence of the metal-free material, **4**. **b**, EDS emission line data at K α (6.40 keV) and K β (7.06 keV) for **4**·[Fe] and the metal-free materials, unwoven linear polymer **3** and 2D molecularly woven polymer **4**. **c–e**, Evidence for long-range ordering in **4**. **c**, SEM image showing well-defined fracture lines caused by putting polymer-supported flakes of **4** under strain. **d**, SEM image showing exfoliation of whole layers caused by putting polymer-supported flakes of **4** under strain. The white arrows in **c** and **d** indicate the direction of strain. **e**, Optical images of a rotating single flake of **4** taken through polarized optical filters showing birefringence. The amount of polarized light that passes through the 2D molecularly woven material is similar every 90° of rotation of the sample (compare images at 20° and 110° (dark) and 60° or 70° and 150° or 160° (bright)), indicative of aligned polymer chains. See Supplementary Video 3 for an animation of the fracturing and delamination processes that resulted in the images in **c** and **d**.

evidenced by infrared (IR) and Raman spectroscopy (Supplementary Figs. 17–19). To compare the effects of strand weaving, a non-woven linear polymer, **3**, was prepared by the oxidation of **2** in the absence of metal salt templates (Fig. 1a, step 2). The molecular chains in both materials are the same AABB homopolymer, consisting of alternating

short aromatic and aliphatic segments, shown for the non-woven linear polymer **3** in Fig. 1a.

Slow evaporation, open to the air, of a solution of freshly prepared [Fe₉2₆](BF₄)₁₈ in toluene:acetonitrile (3:5) led to steady formation (over three days) of a green film and microcrystalline particles on the surfaces of the reaction vessel originally in contact with the solution (Fig. 2c, Supplementary Video 1). Repeated washing of the combined precipitate with acetonitrile afforded **4**·[Fe] as a dark-green solid. This material was insoluble in common organic solvents, similar to the behaviour of a crosslinked polymer. Raman and IR spectroscopy confirmed the absence of unreacted thiol groups in the material (the disulfide region is masked by other signals). Material **4**·[Fe] was treated with potassium cyanide (KCN) in dimethylsulfoxide (DMSO) at room temperature for 16 h to remove Fe(II) and other ions. After isolation and washing with both polar and apolar solvents, a wholly organic molecular fabric, **4**, was isolated as a bright yellow fluorescent material in 72% yield from [Fe₉2₆](BF₄)₁₈ (Fig. 2d, Supplementary Video 1).

Structural characterization of 4

The colour and fluorescence of **4** (Fig. 3a) are indicative of the absence of Fe(II) ions. Elemental analysis was in good agreement with the element stoichiometry required for **4**, and energy-dispersive X-ray spectroscopy (EDS) of **4** confirmed the effectiveness of the demetallation process with baseline values of Fe L α and K α / β emission (Fig. 3b).

Polymers consisting of alternating short aromatic–aliphatic segments rarely form flake-like morphologies, but the demetallated material, **4**, was isolated as large, very thin, flakes and free-standing nanosheets that formed spontaneously without the need for standard exfoliation methods such as sonication or manual grinding¹⁸. The nanosheets were separated from larger flakes by suspension in methanol and centrifugation at 1,500 rpm. The supernatant liquid showed the characteristic Tyndall scattering associated with suspended nanosheets⁴⁰ (Supplementary Fig. 23). Atomic force microscopy (AFM) of samples drop-cast from a methanol suspension onto silicon wafers showed layers of nanosheets with a minimum step height of about 4 nm (Fig. 4c, d, Supplementary Video 2). Note that the horizontal axis of the AFM trace is in micrometres, whereas the vertical axis is in nanometres: the sheets extend for thousands of grid lengths and woven over–under crossings without a change in height. Such extended flat surfaces cannot arise from polymerization in three dimensions, although we do not rule out the formation of some disulfide linkages between layers within a sheet. The scarcity of divots in the AFM traces suggests that within a layer, either the absence of individual tiles is rare or following demetallation the woven strands are able to move to cover small gaps through reptation (slithering movements of regions of the polymer chains within the weave)⁴¹. Sometimes, wrinkles were observed in the molecular fabric as an internal region detached and rose up from the substrate (Fig. 4c), similar to features previously observed⁴² with 2D graphene sheets. As a result of the process used to promote tessellation, most of the sheets were present in stacks or clusters (Supplementary Fig. 25a), but occasionally, an isolated 4-nm-thick sheet could be imaged directly on the surface (Supplementary Fig. 25b).

The thin flat nanosheets were also observed by scanning electron microscopy (SEM) (Fig. 4a, b) and optical microscopy (Supplementary Fig. 24) and, again, suggest well-ordered domains brought about by effective tiling of the parent grids. Short-range order refers to the regular arrangement of atoms over a short distance, usually one or two atom spacings, such as within the unit cell of crystals. Regularity repeated over greater distances—for example, parallel arrangements of polymer chains or mesogens in liquid crystals—is termed long-range order⁴³. Long-range orientational order of polymer chains, often brought about in films and fibres by mechanical processing, can be demonstrated by birefringence⁴³. The flakes of **4** show strong birefringence with maxima every 90° of rotation, confirming long-range

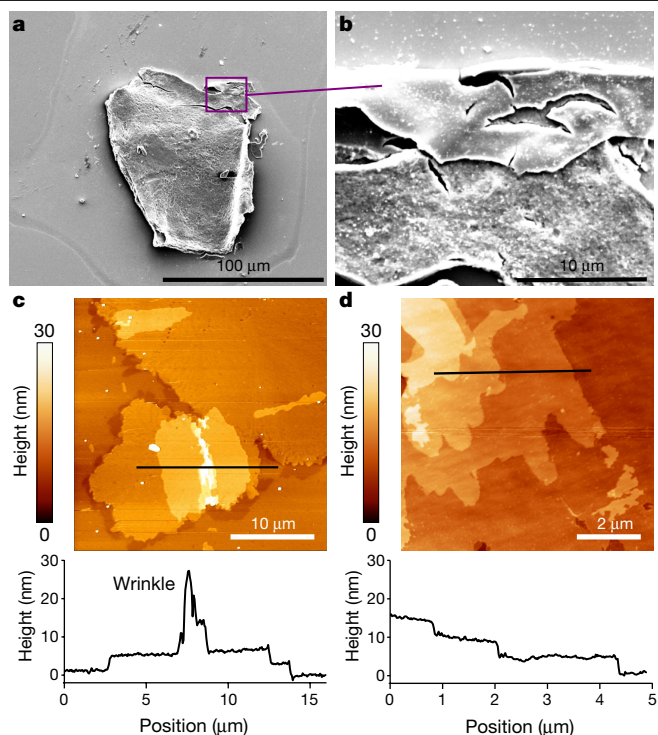


Fig. 4 | Microscopy imaging of layered 2D molecularly woven fabric 4. **a**, SEM image of an individual large flake. **b**, SEM image of a region at higher magnification, showing the thin layered structure. **c**, AFM image of layered nanosheets of **4** dropcast onto Si/SiO₂ (top) with a line profile (horizontal black line, top) showing consistent 4 nm step heights (bottom). **d**, AFM image and line profile of three stacked sheets. The regular height of the surface indicates that the interwoven 2D material generally lies flat and extended, but the image in **c** shows a height change corresponding to a wrinkle in the woven molecular fabric. The SEM and AFM images show the flat surface of the material extending in two dimensions for tens of micrometres in the 2D sheets, corresponding to tens of thousands of over–under crossings for each woven strand. See Supplementary Video 2 for an animation of the AFM imaging of a flat layered sheet.

order and domains of aligned polymer strands (Fig. 3e, Supplementary Information section 1.21). The birefringence data are consistent with the box-weave-strand arrangement proposed for **4**. By contrast, no birefringence was observed for the unwoven linear polymer **3**. Consequences of the long-range order of **4** were apparent in *in situ* deformation caused by applying strain to flakes deposited on a flexible polyester support. The cracking that occurs along clear boundary lines (Fig. 3c) and the slipping between layers (Fig. 3d) are indicative of a material with long-range order and is reminiscent of the response of macroscopic woven textiles to mechanical stress (Supplementary Video 3).

Small-angle X-ray scattering (SAXS) analysis of the metal-coordinated material **4**·[Fe] also shows long-range ordering, with a *d*-spacing (the distance between the aligned chains that gives rise to diffraction) consistent with the size of the parent grid (Supplementary Fig. 32). The wide-angle X-ray scattering (WAXS) of powders of **3** and **4** are similar (Supplementary Fig. 33), showing two broad peaks: one at around $2\theta \approx 25^\circ$ (2θ is the angle between the diffracted X-ray and the incident beam; a value of 25° is typically associated with aliphatic–aliphatic chain spacing) and the other at $2\theta \approx 19^\circ$ (aromatic–aromatic chain spacing). Such like-with-like phase separation of flexible and rigid segments is typical of block copolymers, and the observation that it occurs for **4** suggests that the registry of the aligned strands in the weave is generally maintained in the demetallated 2D molecularly woven material. If strand registry was not conserved, a single, very broad, peak would be expected. The breadth of the two peaks corresponding to aliphatic–aliphatic and aromatic–aromatic

chain spacings (the 2θ values indicate these to be on average about 0.36 nm and about 0.48 nm, respectively) confirm that, despite registry being maintained, every monomer unit does not have exactly the same conformation and intermolecular interactions along the strand. This is unsurprising for a material that is relatively loosely woven from flexible chains aligned through general van der Waals and aromatic stacking interactions. WAXS patterns consisting of broad overlapping peaks showing a similar degree of short-range order have been reported⁴⁴ for poly(amide-*block*-aramid) alternating block copolymers built from similarly short aliphatic and aromatic units (Supplementary Fig. 34). The flakes of **4** were also imaged using transmission electron microscopy (Supplementary Figs. 30, 31). The electron diffraction patterns consist of streaked rings with diameters corresponding to *d*-spacings in the range 0.38–0.48 nm, showing the same degree of short-range ordering of the aliphatic and aromatic units as the WAXS analysis.

Taken together, the characterization data confirm the layered woven architecture of **4**:

(1) The strands in the model grid [Fe₉1₆](BF₄)₁₈ were established as woven by X-ray crystallography (Fig. 1). The strands in the tile used for tessellation, [Fe₉2₆](BF₄)₁₈, were confirmed as woven from the similarity of the characterization data (NMR, mass spectrometry and so on) of [Fe₉1₆](BF₄)₁₈ and [Fe₉2₆](BF₄)₁₈.

(2) IR and Raman spectroscopy confirmed that polymerization of the thiols is complete in both **4**·[Fe] and **4** (Supplementary Figs. 17–19).

(3) AFM and SEM showed that polymerization of the tiles occurs solely in two dimensions, not three, with tessellation over large domains leaving no obvious grid-sized gaps within a sheet (although any small gaps in **4**·[Fe] might be filled in **4** through strand movement following demetallation; Supplementary Information section 1.19). Although polymers consisting of alternating short aromatic–aliphatic segments do not generally form flake-like morphologies, AFM showed that the 4-nm-thick sheets of **4** are atomically flat for thousands of grid lengths in two dimensions (Fig. 4c, d, Supplementary Fig. 25b). SEM images showed displaced sheets of 2D molecularly woven fabric **4** that had slid away from others they were apparently stacked with during the formation of **4**·[Fe] (Fig. 3c, d), further confirmation that the sheets are not crosslinked in three dimensions.

(4) EDS confirmed that **4** is demetallated.

(5) The strands were aligned and fixed in place by metal coordination in the grid before polymerization. As polymerization does not remove the metal ions (EDS confirmed their presence in **4**·[Fe]), the strands must still be aligned, as part of the grid, after within-layer polymerization.

(6) After demetallation, when the strands were no longer bound together by metal ions and had some freedom of movement, birefringence showed that the polymer chains were still aligned. The constraints of topology (it is physically impossible for the strands to pass through each other) mean that the aligned polymer chains must still be woven in **4**, with all of the nine strand crossings that originate from each grid still present in the material (other than some possible fraying at the edges).

(7) The like-with-like phase separation revealed by WAXS demonstrates that the registry of the weave is largely maintained in **4**: aromatic chain segments associate with aromatic segments of other chains, aliphatic with aliphatic, with the chain spacings averaging about 0.36 nm and about 0.48 nm, respectively.

(8) The long-range order (woven architecture) is supported by a wealth of other experimental data, including mechanical fracturing under stress at 90° angles in the manner of a macroscopic box-weave textile and delamination under stress, further confirmation of the layered structure of the weave.

Property comparisons of **3** and **4**

To assess the effects of molecular weaving, we compared the properties of linear 1D polymer **3** and the 2D woven polymer **4** using a number

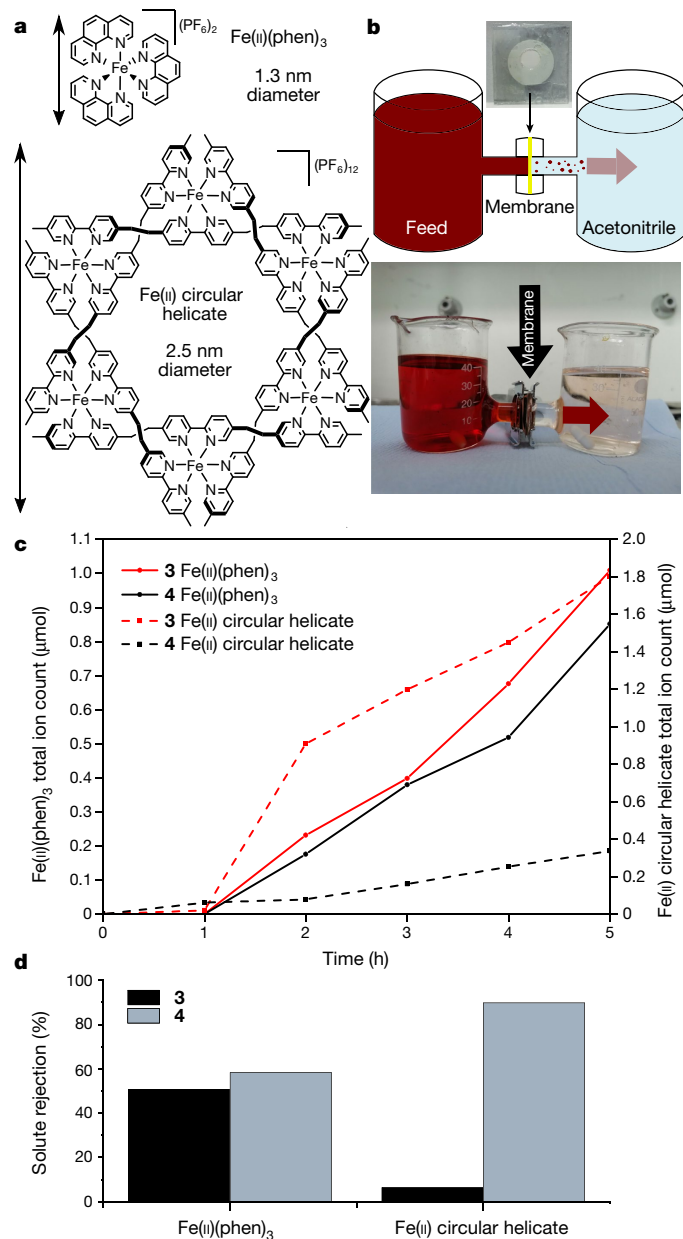


Fig. 5 | Ion permeability studies on PVDF-supported membranes formed from unwoven linear polymer **3 and 2D woven polymer **4**.** **a**, Structures of the Fe(II) complexes used. The arrows indicate the largest diameter for each complex. **b**, Experimental setup for the ion permeation experiments. **c**, Plot comparing the diffusion rates across PVDF-supported membranes of **3** and **4** for Fe(II) complexes of different sizes. **d**, Plot of the relative solute rejection for the different ions across PVDF-supported membranes of **3** and **4** at 5 h. See Supplementary Video 5 for an animation of the ion permeability studies.

of experimental techniques. Preliminary thermogravimetric analysis (TGA) and differential scanning calorimetry (DSC) studies in both air and under an inert atmosphere showed a difference in the thermal stability of the materials. TGA demonstrated that the unwoven linear polymer **3** was more stable than the 2D woven polymer **4**, which showed distinct exotherms at 455 °C and 490 °C under air (Supplementary Fig. 21) that we tentatively assign to the oxidation of the aliphatic and aromatic regions, respectively. It appears that the flake-like morphology of **4**, with a much larger surface-to-volume ratio, facilitates more rapid oxidation.

Determination of the Young's modulus was carried out by AFM using the force–displacement curves obtained at small indentation depths

(Supplementary Fig. 28, Supplementary Video 4). The modulus of **3** and **4** was measured as about 4.5 GPa and about 7.0 GPa, respectively, a substantial difference in stiffness (by way of comparison, typical values⁴³ for nylon, polycarbonate and poly(ethylene terephthalate) (PET) are in the range 2–4 GPa). As would be expected for a woven material, this is consistent with the weaving of the strands in **4** holding them more securely in place than would be the case for a more random, spaghetti-like, arrangement of chains, probably present in **3**.

We also probed the ability of molecular fabric **4** to act as a net—the gaps between the woven warp and weft strands allowing small molecules or ions to pass through but trapping larger ones (Fig. 5, Supplementary Video 5). Syringe-pump filtration of a methanolic suspension of **3** or **4** through polyvinylidene difluoride (PVDF) with 100 nm pores resulted in PVDF-supported membranes of **3** and **4**. SEM analysis of the two membranes showed uniform layers of comparable layer thicknesses, without gaps or deformities (Supplementary Fig. 36). The membranes were used in ion permeability experiments⁴⁵ that determined the rate of ion transfer through each membrane from high-to-low concentration solutions using a small Fe(II)(phen)₃ (phen, phenanthroline) complex (diameter 1.3 nm) and a larger Fe(II) circular helicate (diameter 2.5 nm) (Fig. 5a, b). The PVDF-supported membranes of **3** and **4** allowed permeation of the smaller Fe(II)(phen)₃ complex at similar transfer rates (approximately 2% of the feed concentration over 5 h) and solute rejection values (52–58%; Fig. 5d). However, the membranes had very different rates of transfer for the larger Fe(II) circular helicate (six to ten times faster with **3**; Fig. 5c). The loose tangle of polymer molecules in **3** allows the passage of the large Fe(II) circular helicate cation (solute rejection value 6%; Fig. 5d) while the woven geometry of **4** restricts the number of gaps that are of sufficient size for this larger cation to pass through (solute rejection value 90%; Fig. 5d). Further permeability studies on charged and uncharged species of different shapes and sizes are ongoing.

Discussion

As the difference between stacked^{36,37} and interwoven grids illustrates, the regular repetition of a motif in which two strands simply cross each other is not, in itself, sufficient to generate a mechanically entangled structure. Three-dimensional woven covalent organic frameworks (COFs) have previously been formed¹² from tetrahedral building blocks of stacked bidentate ligands with a single crossing, relying on reticular assembly to generate the entanglements necessary for a weave. However, reticular considerations are insufficient to ensure that a framework of coordination tetrahedra that feature a single crossing generate a lattice that is woven: a weave results only when all adjacent tetrahedra are internally oriented so that the correct ligand ends are connected. Likewise, a recently reported⁴⁶ ring-opening polymerization of a [2]catenane cannot control the crossing sequence nor the orientation of warp and weft strands to ensure that the resulting polymer chains are woven rather than randomly entangled. This contrasts with the approach used to assemble molecularly woven fabric **4**, in which building blocks that are pre-woven are tessellated to extend an already established weave. The resulting demetallated material consists of wholly organic polymer chains with orthogonal warp and weft strands woven in 2D sheets of uniform 4 nm thickness, although the synthetic strategy means that some imperfections in the weave will inevitably occur from chains being incorrectly connected (Supplementary Section 1.19). Following the demetallation, AFM and SEM show individual sheets of the 2D molecularly woven fabric **4** (for example, Supplementary Fig. 25b), demonstrating that the weave is restricted to two dimensions and that the sheets are not crosslinked vertically. Molecularly woven material **4** is formally a 2D woven COF, but it is not made of the short rigid repeat units typical of COFs that promote crystallinity, and **4** has the modest short-range order typical of aligned loosely packed polymer chains (that is, every repeat unit does not simultaneously adopt exactly

the same conformation and intermolecular interactions). It may be easier for materials that are not crystalline, nor derived wholly from rigid constituents, to realize properties that can be imparted by the long-range order of weaving.

Advances in the 'top down' weaving of 1D strands—ranging from threads with diameters measured in millimetres (reeds, plant fibres and so on) to those of a few micrometres (wool, cotton, synthetic polymers and so on)—in two dimensions have underpinned technological progress through the ages¹. As with macroscopic yarns, the weaving of flexible 1D molecular strands into a layered fabric results in a woven material with an array of characteristics and properties that are substantially different to those of the unwoven fibres. The ability to weave polymer chains in two (and potentially three) dimensions by the tessellation or reticulation of pre-woven molecular building blocks offers new opportunities and research directions that combine the fields of polymer structure and topology⁴⁷, 2D materials^{17,18,48} and the molecular-level mechanical bond^{49,50}.

Online content

Any methods, additional references, Nature Research reporting summaries, source data, extended data, supplementary information, acknowledgements, peer review information; details of author contributions and competing interests; and statements of data and code availability are available at <https://doi.org/10.1038/s41586-020-3019-9>.

- Kadolph, S. J. (ed.) *Textiles* 10th edn (Prentice-Hall, 2007).
- Batten, S. R. & Robson, R. Interpenetrating nets: ordered, periodic entanglement. *Angew. Chem. Int. Ed.* **37**, 1460–1494 (1998).
- Carlucci, L., Ciani, G. & Proserpio, D. M. Polycatenation, polythreading and polyknotting in coordination network chemistry. *Coord. Chem. Rev.* **246**, 247–289 (2003).
- Van Calcar, P. M., Olmstead, M. M. & Balch, A. L. Construction of a knitted crystalline polymer through the use of gold(I)–gold(I) interactions. *Chem. Commun.* 1773–1774 (1995).
- Axtell, E. A., III, Liao, J.-H. & Kanatzidis, M. G. Flux synthesis of LiAuS and NaAuS: "Chicken-wire-like" layer formation by interweaving of (AuS)_n^{n−} threads. Comparison with α-HgS and AAuS (A = K, Rb). *Inorg. Chem.* **37**, 5583–5587 (1998).
- Carlucci, L., Ciani, G., Gramaccioli, A., Proserpio, D. M. & Rizzato, S. Crystal engineering of coordination polymers and architectures using the [Cu(2,2'-bipy)]²⁺ molecular corner as building block (bipy = 2,2'-bipyridyl). *CrystEngComm* **2**, 154–163 (2000).
- Li, Y.-H. et al. The first 'two-over/two-under' (2O/2U) 2D weave structure assembled from Hg-containing 1D coordination polymer chains. *Chem. Commun.* 1630–1631 (2003).
- Han, L. & Zhou, Y. 2D entanglement of 1D flexible zigzag coordination polymers leading to an interwoven network. *Inorg. Chem. Commun.* **11**, 385–387 (2008).
- Wu, H., Yang, J., Su, Z.-M., Batten, S. R. & Ma, J.-F. An exceptional 54-fold interpenetrated coordination polymer with 10³-srs network topology. *J. Am. Chem. Soc.* **133**, 11406–11409 (2011).
- Champsaur, A. M. et al. Weaving nanoscale cloth through electrostatic templating. *J. Am. Chem. Soc.* **139**, 11718–11721 (2017).
- Ciengshin, T., Sha, R. & Seeman, N. C. Automatic molecular weaving prototyped by using single-stranded DNA. *Angew. Chem. Int. Ed.* **50**, 4419–4422 (2011).
- Liu, Y. et al. Weaving of organic threads into a crystalline covalent organic framework. *Science* **351**, 365–369 (2016).
- Zhao, Y. et al. A synthetic route for crystals of woven structures, uniform nanocrystals, and thin films of imine covalent organic frameworks. *J. Am. Chem. Soc.* **139**, 13166–13172 (2017).
- Liu, Y. et al. Molecular weaving of covalent organic frameworks for adaptive guest inclusion. *J. Am. Chem. Soc.* **140**, 16015–16019 (2018).
- Lewandowska, U. et al. A triaxial supramolecular weave. *Nat. Chem.* **9**, 1068–1072 (2017).
- Wang, Z. et al. Molecular weaving via surface-templated epitaxy of crystalline coordination networks. *Nat. Commun.* **8**, 14442 (2017).
- Servalli, M. & Schlüter, A. D. Synthetic two-dimensional polymers. *Annu. Rev. Mater. Res.* **47**, 361–389 (2017).
- Mas-Ballester, R., Gómez-Navarro, C., Gómez-Herrero, J. & Zamora, F. 2D materials: to graphene and beyond. *Nanoscale* **3**, 20–30 (2011).
- Busch, D. H. Structural definition of chemical templates and the prediction of new and unusual materials. *J. Incl. Phenom. Macrocycl. Chem.* **12**, 389–395 (1992).
- Hubin, T. J. & Busch, D. H. Template routes to interlocked molecular structures and orderly molecular entanglements. *Coord. Chem. Rev.* **200–202**, 5–52 (2000).
- Cockriel, D. L. et al. The design and synthesis of pyrazine amide ligands suitable for the "tiles" approach to molecular weaving with octahedral metal ions. *Inorg. Chem. Commun.* **11**, 1–4 (2008).
- Wadhwa, N. R., Hughes, N. C., Hachem, J. A. & Mezei, G. Metal-templated synthesis of intertwined, functionalized strands as precursors to molecularly woven materials. *RSC Adv.* **6**, 11430–11440 (2016).
- Mena-Hernando, S. & Pérez, E. M. Mechanically interlocked materials. Rotaxanes and catenanes beyond the small molecule. *Chem. Soc. Rev.* **48**, 5016–5032 (2019).
- Forgan, R. S., Sauvage, J.-P. & Stoddart, J. F. Chemical topology: complex molecular knots, links, and entanglements. *Chem. Rev.* **111**, 5434–5464 (2011).
- Ayme, J.-F., Beves, J. E., Campbell, C. J. & Leigh, D. A. Template synthesis of molecular knots. *Chem. Soc. Rev.* **42**, 1700–1712 (2013).
- Sauvage, J.-P. From chemical topology to molecular machines (Nobel Lecture). *Angew. Chem. Int. Ed.* **56**, 11080–11093 (2017).
- Dietrich-Buchecker, C. O. & Sauvage, J.-P. A synthetic molecular trefoil knot. *Angew. Chem. Int. Ed. Engl.* **28**, 189–192 (1989).
- Chichak, K. S. et al. Molecular Borromean rings. *Science* **304**, 1308–1312 (2004).
- Guo, J., Mayers, P. C., Breault, G. A. & Hunter, C. A. Synthesis of a molecular trefoil knot by folding and closing on an octahedral coordination template. *Nat. Chem.* **2**, 218–222 (2010).
- Ayme, J.-F. et al. A synthetic molecular pentafoil knot. *Nat. Chem.* **4**, 15–20 (2012).
- Prakasam, T. et al. Simultaneous self-assembly of a [2]catenane, a trefoil knot, and a Solomon link from a simple pair of ligands. *Angew. Chem. Int. Ed.* **52**, 9956–9960 (2013).
- Wood, C. S., Ronson, T. K., Belenguer, A. M., Holstein, J. J. & Nitschke, J. R. Two-stage directed self-assembly of a cyclic [3]catenane. *Nat. Chem.* **7**, 354–358 (2015).
- Danon, J. J. et al. Braiding a molecular knot with eight crossings. *Science* **355**, 159–162 (2017).
- Zhang, L. et al. Stereoselective synthesis of a composite knot with nine crossings. *Nat. Chem.* **10**, 1083–1088 (2018).
- Leigh, D. A. et al. Tying different knots in a molecular strand. *Nature* **584**, 562–568 (2020).
- Ruben, M., Rojo, J., Romero-Salguero, F. J., Uppadine, L. H. & Lehn, J.-M. Grid-type metal ion architectures: functional metallosupramolecular arrays. *Angew. Chem. Int. Ed.* **43**, 3644–3662 (2004).
- Dawe, L. N., Abedin, T. S. M. & Thompson, L. K. Ligand directed self-assembly of polymetallic [n × n] grids: rational routes to large functional molecular subunits? *Dalton Trans.* 1661–1675 (2008).
- Leigh, D. A. et al. A molecular endless (7₂) knot. *Nat. Chem.* <https://doi.org/10.1038/s41557-020-00594-x> (2020).
- Pakula, A. A. & Simon, M. I. Determination of transmembrane protein structure by disulfide cross-linking: the *Escherichia coli* Tar receptor. *Proc. Natl. Acad. Sci. USA* **89**, 4144–4148 (1992).
- Sakamoto, R. et al. Coordination nanosheets (CONASHs): strategies, structures and functions. *Chem. Commun.* **53**, 5781–5801 (2017).
- de Gennes, P. G. Reptation of a polymer chain in the presence of fixed obstacles. *J. Chem. Phys.* **55**, 572–579 (1971).
- Zhu, W. et al. Structure and electronic transport in graphene wrinkles. *Nano Lett.* **12**, 3431–3436 (2012).
- Young, R. J. & Lovell, P. A. *Introduction to Polymers* 3rd edn (CRC Press, 2011).
- de Ruijter, C., Mendes, E., Boerstoel, H. & Picken, S. J. Orientational order and mechanical properties of poly(amide-block-aramid) alternating block copolymer films and fibers. *Polymer* **47**, 8517–8526 (2006).
- Kontturi, K., Murtomäki, L. & Manzanares, J. A. *Ionic Transport Processes in Electrochemistry and Membrane Science* (Oxford Univ. Press, 2014).
- Li, G. et al. Woven polymer networks via the topological transformation of a [2]catenane. *J. Am. Chem. Soc.* **142**, 14343–14349 (2020).
- Hawker, C. J. & Wooley, K. L. The convergence of synthetic organic and polymer chemistries. *Science* **309**, 1200–1205 (2005).
- Sakamoto, J., van Heijst, J., Lukin, O. & Schlüter, A. D. Two-dimensional polymers: just a dream of synthetic chemists? *Angew. Chem. Int. Ed.* **48**, 1030–1069 (2009).
- Wu, Q. et al. Poly[n]catenanes: synthesis of molecular interlocked chains. *Science* **358**, 1434–1439 (2017).
- Stoddart, J. F. Dawning of the age of molecular nanotopology. *Nano Lett.* **20**, 5597–5600 (2020).

Publisher's note Springer Nature remains neutral with regard to jurisdictional claims in published maps and institutional affiliations.

© The Author(s), under exclusive licence to Springer Nature Limited 2020

Methods

Synthesis of 3×3 interwoven grid $[\text{Fe}_9\text{2}_6](\text{BF}_4)_{18}$

Ligand **2** (49.7 mg, 43.1 μmol) and $\text{Fe}(\text{BF}_4)_2 \cdot 6\text{H}_2\text{O}$ (21.8 mg, 1.5 equiv., 64.6 μmol) were suspended in acetonitrile (6.2 ml) and toluene (3.7 ml) in a microwave vessel under N_2 atmosphere. The mixture was heated at 120 °C in a microwave for 20 h. After cooling, the mixture was diluted with diethyl ether and the resulting dark-green precipitate filtered onto Celite, washed with diethyl ether and redissolved in acetonitrile. After solvent evaporation, the resulting dark green powder was kept under nitrogen (46 mg, 4.5 μmol , 62% yield) or alternatively dissolved in acetonitrile for immediate use. For characterization data, see Supplementary Information.

Tessellation and polymerization of $[\text{Fe}_9\text{2}_6](\text{BF}_4)_{18}$ to form $4 \cdot [\text{Fe}]$

Freshly prepared $[\text{Fe}_9\text{2}_6](\text{BF}_4)_{18}$ (12.2 mg, 1.2 μmol based on 100% conversion from ligand **2**) was dissolved in a mixture of toluene (1 ml) and acetonitrile (1.67 ml). After slow precipitation and concomitant polymerization in air over three days, a green film and microcrystalline particles had collected on the surfaces of the reaction vessel. This material was washed repeatedly with acetonitrile to give the product as a dark-green solid (8.0 mg, 66%). See Supplementary Information for characterization data.

Demetallation of $4 \cdot [\text{Fe}]$ to form wholly organic 2D molecularly woven fabric **4**

Material $4 \cdot [\text{Fe}]$ (8.0 mg) was suspended in 3 ml DMSO with 15.0 mg KCN (300 equiv., approximately five times the amount required to fully complex all of the Fe(II) cations). The dark-green turbid solution was left at room temperature for 16 h. The resulting turbid dark-orange solution was diluted to 5 ml with DMSO and centrifuged. The supernatant was discarded; the orange solid was suspended in 5 ml DMSO and centrifuged again. The process was repeated until the DMSO was colourless (typically four times) and then twice with ethanol and other solvents. The solid was dried under vacuum and the material was isolated as a

pale-yellow–orange powder **4** (4.6 mg, 72% yield). See Supplementary Information for characterization data.

Data availability

The data that support the findings of this study are available within the paper and its Supplementary Information, or are available from the Mendeley data repository (<https://data.mendeley.com/>) with the identifier <https://doi.org/10.17632/zkt5km82r2.2>.

Acknowledgements We thank the Engineering and Physical Sciences Research Council (EPSRC; EP/P027067/1), the European Research Council (ERC; Advanced Grant no. 786630), and the Defense Advanced Research Projects Agency (DARPA; Co-operative Agreement W911NF-17-2-0148) for funding; with networking contributions from the COST Action CA17139, EUTOPIA. The views, opinions and/or findings expressed are those of the authors and should not be interpreted as representing the official views or policies of the Department of Defense or the US Government. We also thank the Diamond Light Source (UK) for synchrotron beam time on I19 (XR029), the University of Manchester, Department of Chemistry microanalysis and mass spectrometry services, the Henry Royce Institute for Advanced Materials (funded through EPSRC grants EP/R00661X/1 and EP/P025021/1) for the use of facilities, S. Jantzen/Biocinematics for the video animations, and S. J. Rowan (University of Chicago) and R. P. Sijbesma (Eindhoven University) for comments that improved the draft manuscript. D.A.L. is a Royal Society Research Professor.

Author contributions D.P.A., L.I.P., J.-F.L. and Y.S. carried out the synthesis and general characterization studies. G.F.S.W. solved the crystal structure of $[\text{Fe}_9\text{1}_6](\text{BF}_4)_{18}$. Z.L., C.A.M. and R.J.Y. carried out the AFM studies. Z.L. and R.J.Y. performed the Young's modulus, polarized optical microscope and deformation experiments. S.J.H. conducted the transmission electron microscopy studies, and R.A.W.D. and P.R.C.K. conducted the ion permeation studies. D.A.L. directed the research. All authors contributed to the analysis of the results and the writing of the manuscript. Authors are listed alphabetically in view of the broad range of experimental techniques used in this study.

Competing interests The authors declare no competing interests.

Additional information

Supplementary information is available for this paper at <https://doi.org/10.1038/s41586-020-3019-9>.

Correspondence and requests for materials should be addressed to D.A.L.

Peer review information *Nature* thanks the anonymous reviewer(s) for their contribution to the peer review of this work.

Reprints and permissions information is available at <http://www.nature.com/reprints>.